energies

MDPI

Article

A Computational Fluid Dynamics Study of Laminar Forced Convection Improvement of a Non-Newtonian Hybrid Nanofluid within an Annular Pipe in Porous Media

Hesam Moghadasi [1,2], Mohamad Bayat [2], Ehsan Aminian [1], Jesper H. Hattel [2] and Mahdi Bodaghi [3,*]

[1] School of Mechanical Engineering, Iran University of Science and Technology (IUST), Narmak, Tehran 16846-13114, Iran
[2] Department of Mechanical Engineering, Technical University of Denmark, 2800 Kongens Lyngby, Denmark
[3] Department of Engineering, School of Science and Technology, Nottingham Trent University, Nottingham NG11 8NS, UK
* Correspondence: mahdi.bodaghi@ntu.ac.uk

Abstract: Porous inserts and nanofluids are among the conventional methods for the amelioration of heat transfer in industrial systems. The heat transfer rate could also be improved by utilizing porous substances with a higher thermal conductivity in these systems. This research work presents a two-dimensional (2D) numerical examination of the laminar forced convection of an Al_2O_3-CuO-carboxy methyl cellulose (CMC) non-Newtonian hybrid nanofluid within an annular pipe in a porous medium. The porous medium was inserted within two inner or outer wall cases. For hybrid nanofluid flow modeling in porous media, a Darcy–Brinkman–Forchheimer formulation was employed. Additionally, a power-law technique was utilized as a fluid viscosity model for the considered non-Newtonian fluid. The governing equations were discretized according to the finite volume method (FVM) using the computational fluid dynamics (CFD) software package ANSYS-FLUENT. The cylinder walls' thermal boundary conditions were exposed to a constant heat flux. For various Darcy numbers, the impacts of different volume fractions of the hybrid nanofluid (0% to 5%), the total Nusselt number, the pressure drop, and the performance number (PN) were evaluated. The outcomes indicate that the heat transfer coefficient increases considerably with a decrease in the Darcy number (0.1 to 0.0001), as well as with an increase in the porous thickness ratio. Moreover, it was found that the nanoparticles' increased volume fraction would ameliorate the heat transfer and, more considerably, the PN factor. Furthermore, according to the outcomes in both cases I and II for a constant porous thickness ratio and Darcy number ($r_p = 1, Da = 0.0001$) and a high volume fraction ($\varphi = 5\%$), the maximum total Nusselt number reached 1274.44. Moreover, applying a volume fraction of 5% with $Da = 0.1$ and $r_p = 1$ reached the highest value of the PN index equal to 7.61, which is augmented as roughly 88% compared to the case of a zero volume fraction.

Keywords: CFD; heat transfer; non-Newtonian hybrid nanofluid; volume fraction; porous media

check for updates

Citation: Moghadasi, H.; Bayat, M.; Aminian, E.; Hattel, J.H.; Bodaghi, M. A Computational Fluid Dynamics Study of Laminar Forced Convection Improvement of a Non-Newtonian Hybrid Nanofluid within an Annular Pipe in Porous Media. *Energies* **2022**, *15*, 8207. https://doi.org/10.3390/en15218207

Academic Editors: Jianzhong Lin, Qiang Zhou, Zhenjiang You, Fubing Bao and Kun Zhou

Received: 21 October 2022
Accepted: 31 October 2022
Published: 3 November 2022

Publisher's Note: MDPI stays neutral with regard to jurisdictional claims in published maps and institutional affiliations.

Copyright: © 2022 by the authors. Licensee MDPI, Basel, Switzerland. This article is an open access article distributed under the terms and conditions of the Creative Commons Attribution (CC BY) license (https://creativecommons.org/licenses/by/4.0/).

1. Introduction

The heat transfer efficiency can be drastically ameliorated using nanofluid media. Because of their high thermal conductivity, nanofluids play a huge role in the heat transfer in different energy conversion applications such as energy storage, solar equipment, heat exchangers, radiators, automobiles, and various medical areas [1–3]. As a result, heat transfer and nanofluid flow have been widely investigated both numerically and experimentally [4–6]. Recently, superior thermophysical features have been found for a novel group of fluids, i.e., the so-called hybrid nanofluids. Compared to common heat transfer fluids, hybrid nanofluids offer better thermophysical properties as well as a more robust thermal performance [7], and hence, they have been the focus of several experimental and numerical investigations [8–11].Tahir and Mital [12] numerically examined the forced

convection heat transfer within the laminar flow of a water-aluminum oxide nanofluid in a channel with a round cross-section. They compared the impacts of the volume fraction, the size of nanoparticles, and the Reynolds number on the improvement in the nanofluid's heat transfer and found the Reynolds number to be the most important of the three. In another work, Moshizi et al. [13] assessed the pressure drop and heat transfer of an Al_2O_3-water nanofluid within a tube exposed to a constant heat flux. They showed an improved ratio of the pressure gradient to the heat transfer coefficient as a result of the slip velocity at the tube walls.

The viscosity and thermal conductivity of the Al_2O_3-Cu/H_2O hybrid nanofluid were studied by Suresh et al. [14], in which they found these two parameters to be improved by increasing the nanoparticles' volume concentrations. To evaluate the impact of nanofluids on laminar forced convection, the nanofluid (water-based Al_2O_3) was compared with the hybrid nanofluid (Al_2O_3-Cu) of Moghadassi et al. [15], who reported a substantially improved heat transfer coefficient for the employed hybrid nanofluid. Numerous studies have recently evaluated the heat transfer in porous media [16,17]. In the last ten years, the co-application of porous media and nanofluids for enhancing heat transfer has received increased attention. Uphill et al. [18] assessed the nanofluids' flow through porous media and revealed that nanofluids comprising particles smaller than 60 nm had improved flow in timber. The influences of temperature and the volume fraction of particles on hybrid nanofluids comprising multiwalled carbon nanotubes and iron oxide nanoparticles suspended in a water-base fluid were scrutinized experimentally by Sundar et al. [19]. They performed the experiments at temperatures of 20–60 °C and volume fractions of more than 3%. Specifically, they found an increase of 31% in the thermal conductivity at the temperature of 60 °C and a volume fraction of 3%. Esfe et al. [20] experimentally studied the influence of the concentration and temperature of titanium and copper oxide nanoparticles at 30–60 °C and volume fractions at a maximum of 2%. A hybrid mixture of water and ethylene glycol was selected as the base fluid. They found a 44% increase in the thermal conductivity for a 2% volume fraction at 60 °C. A double-pipe-type heat exchanger occupied with nanofluids and porous baffles was investigated by Targui and Kahalerras [21]. The effects of the nanoparticles' volume fraction, as well as their type, on the system operation were evaluated through nanofluid single-phase modeling in a porous medium via the Darcy–Brinkman–Forchheimer approach. They found that the heat transfer gain was mainly dependent on the solid volume fraction rather than the nanoparticles' type.

The non-Newtonian nanofluids have also been intensively studied to improve heat transfer in fluid flows [22–24]. According to the studies, most nanofluids are non-Newtonian, which is mainly due to the agglomeration of nanoparticles [25]. Hatami and Ganji [26] investigated the heat transfer and fluid flow for a non-Newtonian nanofluid, which flows within a porous medium between two coaxial cylinders. Results suggested that augmenting the thermophoresis variable increased the general temperature level in the whole domain. Shahsavar et al. [27] evaluated the heat transfer performance of a non-Newtonian hybrid nanofluid in a double-pipe mini-channel heat exchanger by considering the temperature-dependent viscosity and thermal conductivity numerically. Furthermore, they showed that the non-Newtonian hybrid nanofluid has a lower pumping power, pressure drop, and performance evaluation criterion, whereas the opposite is correct for the heat transfer rate, the overall heat transfer coefficient, and the effectiveness in comparison with the Newtonian hybrid nanofluid.

Numerous examples of a heat transfer improvement achieved by applying either porous media or nanofluids, or the combination of the two, were presented in the aforementioned literature study. However, forced convection and laminar flow in a non-Newtonian hybrid nanofluid flowing within an annular pipe in a porous medium have been scarcely studied. Therefore, in the current work, a computational fluid dynamics (CFD) study is carried out on the laminar fluid flow behavior and the associated heat transfer of the non-Newtonian carboxy methyl cellulose (CMC) hybrid nanofluid with a volume fraction

range from 0% to 5% in a two-dimensional (2D) axisymmetric annular pipe. A porous medium is considered for the inner or outer wall, and this is exposed to a constant heat flux; see Figure 1. To analyze the rheological performance of the operating nanofluid, a power law with the usual power-law and consistency indices was used for all volume fractions. Studying the effects of the volume fraction, Darcy number, porous thickness ratio, total Nusselt number, pressure drop, and performance number (PN) is the research aim and question which should be answered in this work.

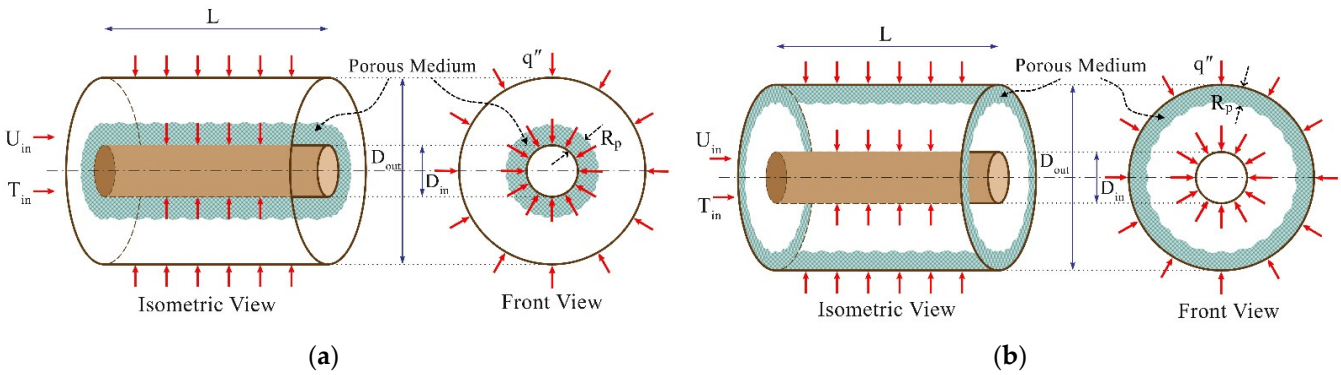

Figure 1. Schematic geometry of the problem. (**a**) Case I, porous medium in the inner wall. (**b**) Case II, porous medium in the outer wall.

2. Problem Description

2.1. Configuration

Figure 1 schematically describes the configuration of the considered case study. The outer diameter is $D_{out} = 0.1$ m, the channel length is $L = 3$ m, and the inner diameter is $D_{in} = 0.04$ m. The channel walls are subject to a constant heat flux of $q'' = 500$ W·m^{-2}. Nanoparticles (particle diameter of 38 nm) are in thermal equilibrium at all times and throughout the domain. The nanofluid's inlet temperature is $T_{in} = 300$ K. The volume fraction and Darcy number ranges are $0\% \leq \varphi \leq 5\%$ and $0.0001 \leq Da \leq 0.1$. The Reynolds number was assumed to be 500 for predicting the fluid behavior and the non-Newtonian fluid's laminar-flow heat transfer coefficient. The details of the geometric features and operating parameters are tabulated in Table 1. As indicated earlier, the heat transfer of a non-Newtonian hybrid nanofluid flowing through an annulus pipe, completely or partially filled with a porous cylinder shell and confined within impermeable walls, is assumed for two cases; see Figure 1. In case I, the porous insert from the outer wall of the cylinder with a smaller radius begins to grow, whereas in case II, the porous medium from the inner wall of the cylinder with a larger radius begins to grow. Furthermore, the heat flux is applied to the outer walls of the two cylinders in both cases I and II.

Table 1. Geometrical dimensions and operating parameters of the problem.

Properties	Value	Unit
L	3	m
D_{in}	0.04	m
D_{out}	0.1	m
T_{in}	300	K
q''	500	W·m^{-2}

The porous medium is set to be completely saturated with fluid ($\varepsilon = 0.9$). Furthermore, the selected fluid is supposed to be incompressible, whereas the flow is steady and laminar. Moreover, the thermophysical characteristics of the porous medium and the working fluid were considered to be constant and the porous medium and the working fluid were in local

thermal equilibrium throughout the whole domain. Additionally, radiative heat transfer and gravity were ignored.

2.2. Theoretical Formulation

The governing equations for a 2D steady-state flow based on the conservation of mass, energy and momentum were considered based on refs. [28,29]. Additionally, some important dimensionless numbers are represented in Equation (1):

$$Re = \frac{\rho_f U_{in} D_h}{\mu_f} \quad , \quad Nu = \frac{D_h \left(\frac{\partial T}{\partial y}\right)_{wall}}{T_{wall} - T_b} \quad , \quad Da = \frac{K}{D_h^2} \quad , \quad r_p = \frac{R_p}{R} \tag{1}$$

In Equation (1), Nu, Re, Da, and r_p represent the Nusselt, Reynolds, and Darcy numbers, and the porous thickness ratio, respectively. The efficient thermal conductivity of the applied fluid in porous media is calculated using Equations (2) and (3) [30]:

$$k_m = (1 - \varphi)k_f + \varphi k_{np} \tag{2}$$

$$k_{eff} = (1 - \varepsilon)k_p + \varepsilon k_m \tag{3}$$

where m, p, np, f, and eff stand for mixture, porous, nanoparticle, fluid, and effectiveness.

2.3. Thermophysical Properties of the Nanofluid

It is worth noting that the base fluid is a non-Newtonian fluid with average thermophysical properties that can be obtained as follows [31]:

$$\rho_{nf} = (1 - \varphi)\rho_{bf} + \varphi\rho_{np} \tag{4}$$

$$c_{p,nf} = \frac{(1 - \varphi)\rho_{bf}c_{p,bf} + \varphi\rho_{np}c_{p,np}}{\rho_{nf}} \tag{5}$$

$$\mu_f = m\dot{\gamma}^{n-1} \tag{6}$$

where bf, nf, and np correspond to the base fluid, nanofluid, and nanoparticle, respectively. In Equation (6), m indicates the consistency index, n denotes the power-law index, and $\dot{\gamma}$ is the shear rate. The thermal conductivity and the power-law and consistency indices expressed in Equation (5) are provided in Table 2 for the considered nanofluid samples, for different values of φ (%).

Table 2. The thermal conductivity and applied indices of the non-Newtonian nanofluid for different volume fractions adopted from [32].

φ (%)	k_f (W·m^{-1}·K^{-1})	m	n
0	0.613	0.145	0.542
1	0.616	0.142	0.537
2	0.652	0.125	0.558
3	0.764	0.114	0.571
4	0.826	0.110	0.586
5	0.9036	0.103	0.594

2.4. Thermophysical Characteristics of the Hybrid Nanofluid

In the present work, copper oxide and aluminum particles were dispersed in the CMC base fluid. The effective values of density, heat capacity, and thermal diffusivity of the applied hybrid nanofluid are calculated as follows:

$$\rho_{hnf} = (1 - \varphi)\rho_{bf} + \varphi\rho_{np} \tag{7}$$

$$(\rho c_p)_{hnf} = (1-\varphi)(\rho c_p)_{bf} + \varphi(\rho c_p)_{np} \tag{8}$$

$$\alpha_{hnf} = \frac{k_{hnf}}{(\rho c_p)_{hnf}} \tag{9}$$

where bf, np, and hnf indices represent the base fluid, nanoparticles, and hybrid nanofluid, respectively. The thermal conductivity coefficient and nanofluid viscosity were calculated using Maxwell and Brinkman formulations as follows [33]:

$$k_{hnf} = \frac{k_{np} + (n-1)k_{bf} - (n-1)\left(k_{bf} - k_{np}\right)\varphi}{k_{np} + (n-1)k_{bf} + \left(k_{bf} - k_{np}\right)\varphi} k_{bf} \tag{10}$$

$$\mu_{hnf} = \frac{\mu_{bf}}{(1-\varphi)^{2.5}} \tag{11}$$

It is worth noting that in Equation (10), n is assumed to be equal to 3 [33]. The thermophysical characteristics of Al_2O_3 and CuO nanoparticles can be obtained as in [34].

$$\varphi = \varphi_{Al_2O_3} + \varphi_{CuO} \tag{12}$$

$$\rho_{hnp} = \frac{\varphi_{Al_2O_3}\,\rho_{Al_2O_3} + \varphi_{CuO}\,\rho_{CuO}}{\varphi} \tag{13}$$

$$(c_p)_{hnp} = \frac{\varphi_{Al_2O_3}\,(c_p)_{Al_2O_3} + \varphi_{CuO}\,(c_p)_{CuO}}{\varphi} \tag{14}$$

$$k_{hnp} = \frac{\varphi_{Al_2O_3}\,k_{Al_2O_3} + \varphi_{CuO}\,k_{CuO}}{\varphi} \tag{15}$$

Table 3 shows the characteristics of the applied base fluid and nanoparticles. As seen, the nanoparticles have a thermal conductivity much higher in comparison to the base fluid (CMC).

Table 3. The thermophysical features of nanoparticles and CMC (CMC/Al_2O_3- CuO) adopted from [35–38].

Properties	*CMC*	Al_2O_3	*CuO*	*Unit*
c_p	4179	765	540	$J{\cdot}kg^{-1}{\cdot}K^{-1}$
k	0.613	40	18	$W{\cdot}\,m^{-1}{\cdot}K^{-1}$
ρ	997	3970	6500	$kg{\cdot}m^{-3}$
μ	0.000998	-	-	$kg{\cdot}m^{-1}{\cdot}s^{-1}$

2.5. Boundary Conditions

As depicted in Figure 1, a uniform profile in the pipe (300 K) with a steady laminar flow was considered for the simulation. The Reynolds number ($Re = 500$) can be obtained using Equation (1) at the entrance temperature. A constant heat flux ($500\ W{\cdot}m^{-2}$) was included in the thermal boundary conditions at the walls.

2.6. Numerical Solution

The 2D steady-flow CFD model was developed using the commercial software ANSYS-FLUENT as a finite volume-based CFD solver. The convective and diffusive terms were discretized by the second-order upwind and central approaches, respectively. Additionally, the line-by-line approach was selected to solve the algebraic formulations iteratively. Moreover, the semi-implicit approach for the pressure-linked equations (SIMPLE) algorithm was considered in order to solve the pressure–velocity coupling. The separated energy equation was solved upon velocity field convergence (from the momentum and continuity

formulations). The primarily under-relaxation factors of 1, 0.7, and 0.3 were utilized for energy, momentum, and pressure, respectively. Using these three factors, the solution stability was maintained. Furthermore, the relative convergence criterion of momentum conservation, energy, and mass formulations was set at 10^{-5}.

2.7. Mesh Independence Analysis

An important part of the simulation procedure is the mesh generation, since it affects the convergence, time, and solution. It is worth noting that adequately fine grids are needed to assess the steep gradient of the physical properties close to the wall grids. Since these gradients frequently occur close to the wall normally, the regular meshing with radially augmented elements was adjusted (Figure 2). Five different cell sizes were examined, as listed in Table 4, and the Nusselt number (see Equation (1)) was selected as the main criterion for finding the converged mesh configuration. The mesh independence analysis was carried out at Re = 500 for a non-Newtonian fluid with nanoparticles with a diameter of $dp = 38$ nm. As the refinement from 100×2000 to 200×4000 made virtually no change in the Nu, the former was chosen as the main grid for the following calculations; see Table 4.

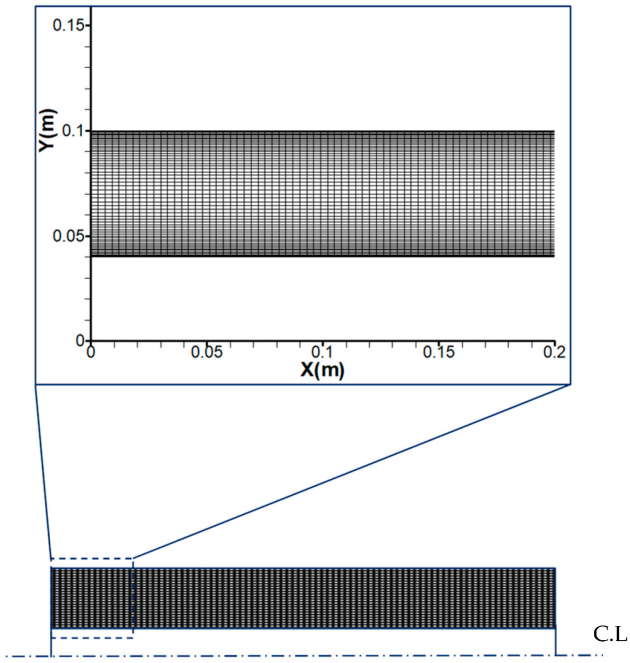

Figure 2. The mesh generated for the present work.

Table 4. Mesh independence for the present study considering different mesh sizes at $Re = 500$.

Mesh Size	Nusselt Number
10×500	17.6
20×750	30.6
50×1000	38.6
100×2000 (*Main Grid*)	40.5
200×4000	40.6

2.8. Model Validation

Following the mesh sensitivity analysis, the actual simulation was conducted. To verify the introduced scheme, the simulation outcomes were compared with values measured by Akbari et al. [39]. The comparison results for temperature revealed a good agreement,

as presented in Figure 3. This validates that the current model's predictions are accurate within the range of the parameters used.

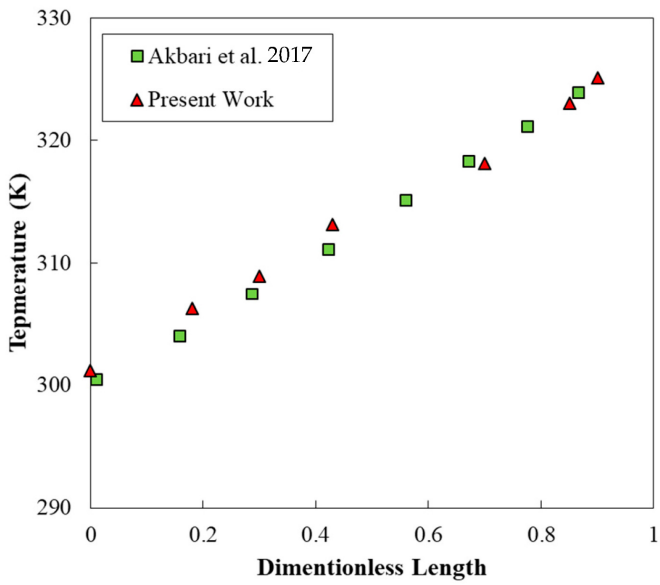

Figure 3. Validating the current solution with the data of Akbari et al. [39].

3. Results and Discussions

Here, the effects of porosity and adding nanoparticles to the base configuration are assessed based on the pressure drop, total Nusselt number, PN, and volume fraction. This is performed to examine the improved heat transfer features and optimum conditions of fluid flow within the annuli in cases I and II, which refer to the porous insert being situated in the inner and outer wall, respectively.

3.1. The Influences of Volume Fraction on Heat Transfer

In Figures 4 and 5a–d, the plot of the total Nusselt number $(Nu = Nu_i + Nu_o)$ versus the porous thickness ratio (r_p) is presented for a range of volume fractions. In these figures, various Darcy numbers were considered for both cases I and II.

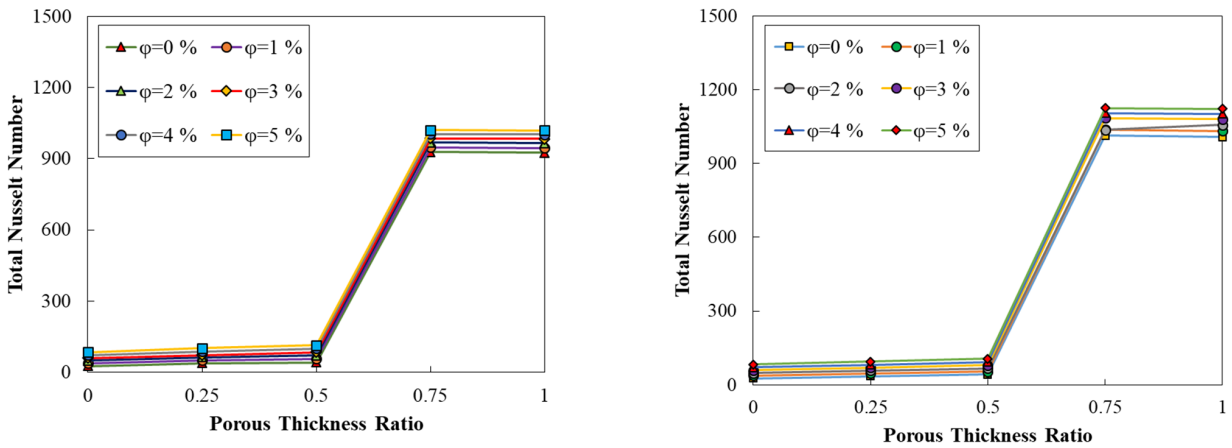

(**a**): $Da = 0.1$ (**b**): $Da = 0.01$

Figure 4. *Cont.*

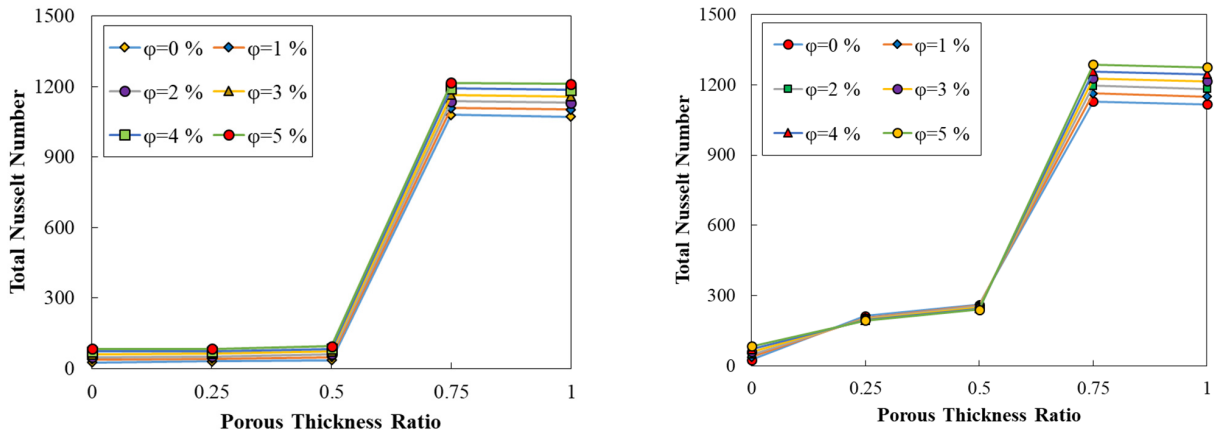

(**c**): $Da = 0.001$ (**d**): $Da = 0.0001$

Figure 4. Total Nusselt number versus porous thickness ratio for diverse volume fractions at different Darcy numbers (case I).

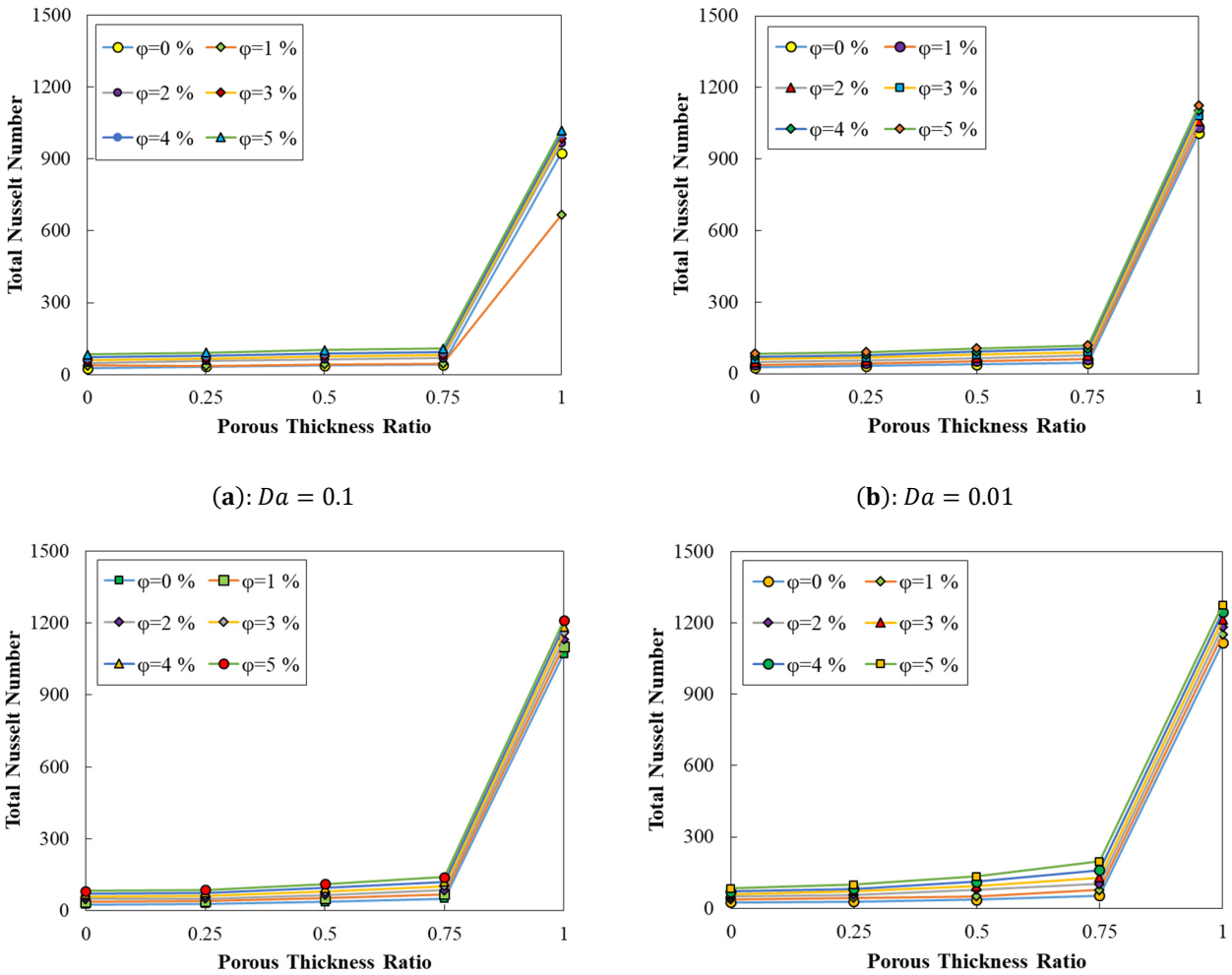

(**a**): $Da = 0.1$ (**b**): $Da = 0.01$

(**c**): $Da = 0.001$ (**d**): $Da = 0.0001$

Figure 5. Total Nusselt number versus porous thickness ratio for diverse volume fractions at different Darcy numbers (case II).

As observed in Figures 4 and 5a–d, improving the porous thickness ratio augmented the heat transfer coefficient and total Nusselt number. Furthermore, decreasing the Darcy number (caused by the medium's reduced permeability) from 0.1 to 0.0001 improved the total Nusselt number (Figures 4 and 5).

The values of total Nusselt numbers at $r_p < 0.5$ for both cases I and II as well as for all Darcy numbers are small, whereas for $r_p \geq 0.5$, the total Nusselt number values increased substantially because of the effect of the porous thickness ratio and increasing the accumulation of fluid near the walls, which led to improving the total Nusselt numbers in both cases.

In Figures 4 and 5, the dependence of the total Nusselt number on the volume fraction of nanoparticles was examined as well. A higher nanoparticle volume fraction results in a better heat transfer coefficient at a constant porous thickness ratio. It is necessary to mention that less permeability leads to more pronounced swelling of the fluid near the walls. This phenomenon results in an augmentation in the velocity gradient that, in turn, leads to a higher heat transfer. In addition, by adding nanoparticles and rising the volume fraction, the thermal conductivity coefficient increases significantly, which leads to a better heat transfer.

By comparing cases I and II for a constant porous thickness ratio $(r_p = 1)$ at $Da = 0.0001$ and at a high volume fraction $(\varphi = 5\%)$, the maximum total Nusselt number reached approximately 1274.44.

3.2. The Impacts of the Darcy Number on the Pressure Drop

Figure 6a,b presents the effects of the Darcy number on the pressure drop considering the maximum volume fraction $(\varphi = 5\%)$. An obvious increasing trend was found for the pressure drop when reducing the Darcy numbers from 0.1 to 0.0001 because of less permeability. Furthermore, as depicted in Figure 6a,b, $Da = 0.0001$ corresponds to the maximum value of the pressure drop for both cases I and II, whereas the minimum pressure drop was obtained when $Da = 0.1$ due to the same mechanism.

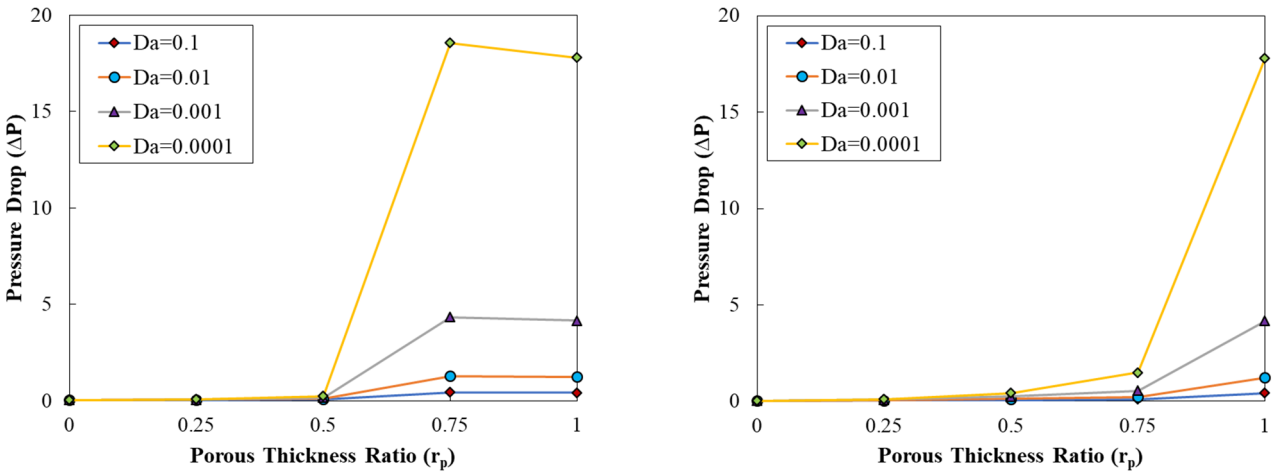

(**a**): Case I (**b**): Case II

Figure 6. Pressure drop versus porous thickness ratio at diverse Darcy numbers for cases I and II, considering $(\varphi = 5\%)$.

It is necessary to mention that less permeability results in more significant fluid congestion close to the walls. This phenomenon leads to a remarkable growth in the velocity gradient and in the pressure drop as well.

By comparing cases I and II in a constant porous thickness ratio $(r_p = 1)$ with a permeable medium $(Da = 0.0001)$ and for a high volume fraction $(\varphi = 5\%)$, the highest pressure drop of $\Delta P = 17.79$ Pa for cases I and II occurred for $\varphi = 5\%$ because of the

non-Newtonian behavior of the fluid, and also because of the accumulation of fluid near the walls in high volume-fraction values.

3.3. The Impacts of Volume Fraction on the Performance Number

The nondimensional variable of Nu/Nu_b represents the Nusselt number ratio at a specific, considered porosity arrangement and the nanoparticle content with the Nusselt number at the nominal condition, where the two Nusselt numbers were determined for the same Reynolds number. This variable could assist in the further clarification of the role of the porosity arrangement or the addition of nanoparticles in enhancing the heat transfer. In general, the heat transfer is improved by the addition of nanoparticles or inserting porous media within the annulus. However, the pressure drop is increased, thus increasing the power consumption. In this regard, for a better physical clarification, the PN parameter can be defined as a function of the pressure drop and Nusselt number ratio as follows [40]:

$$PN = \frac{Nu/Nu_b}{\Delta P/\Delta P_b} \tag{16}$$

where PN is increased by augmenting the Nusselt number and reduced by rising the pressure drop. In Figures 7 and 8a–d, the PN values were calculated for various volume fractions (0% to 5%) as a function of the porous thickness ratio for cases I and II.

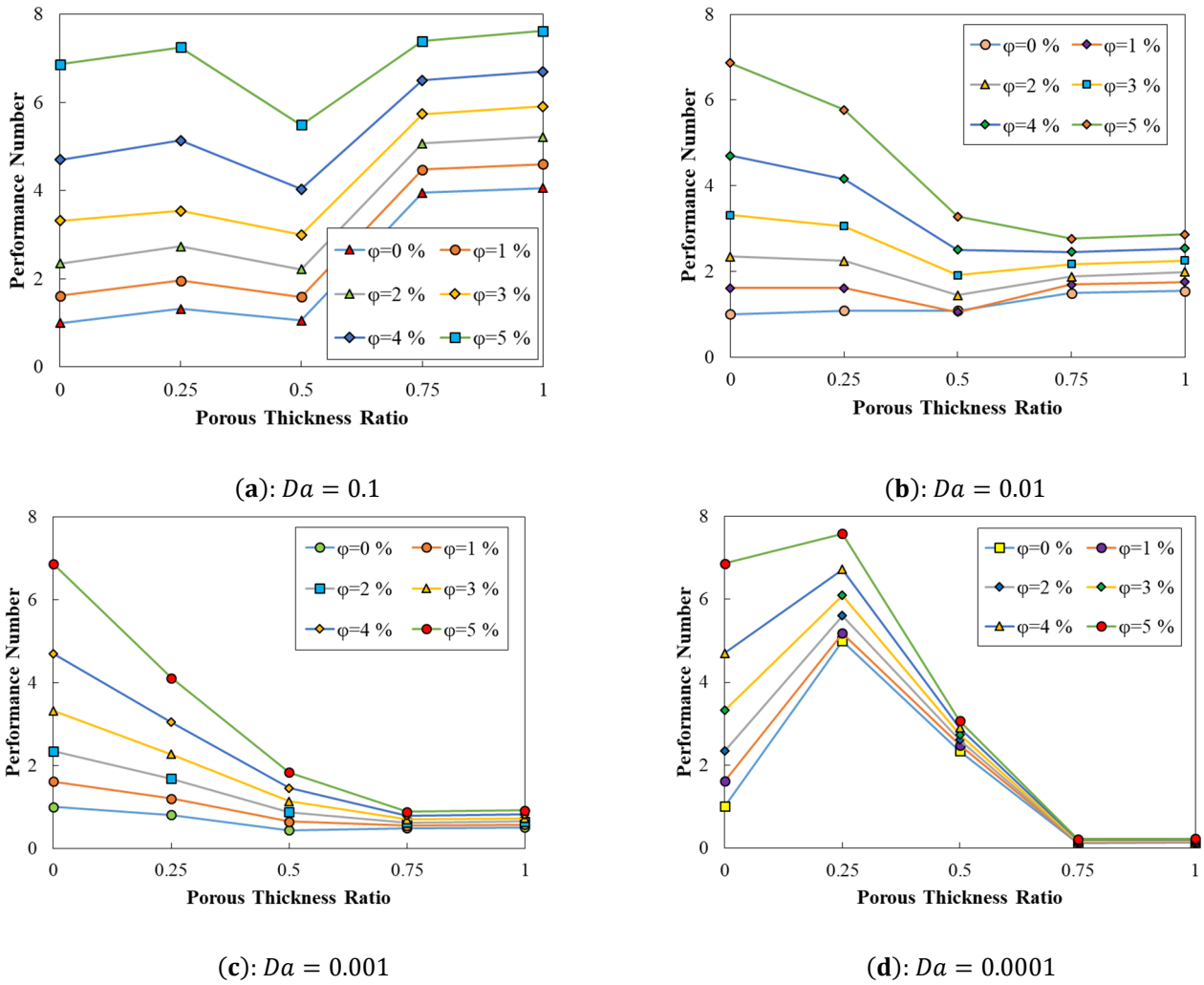

Figure 7. Performance number versus porous thickness ratio for diverse volume fractions at different Darcy numbers (case I).

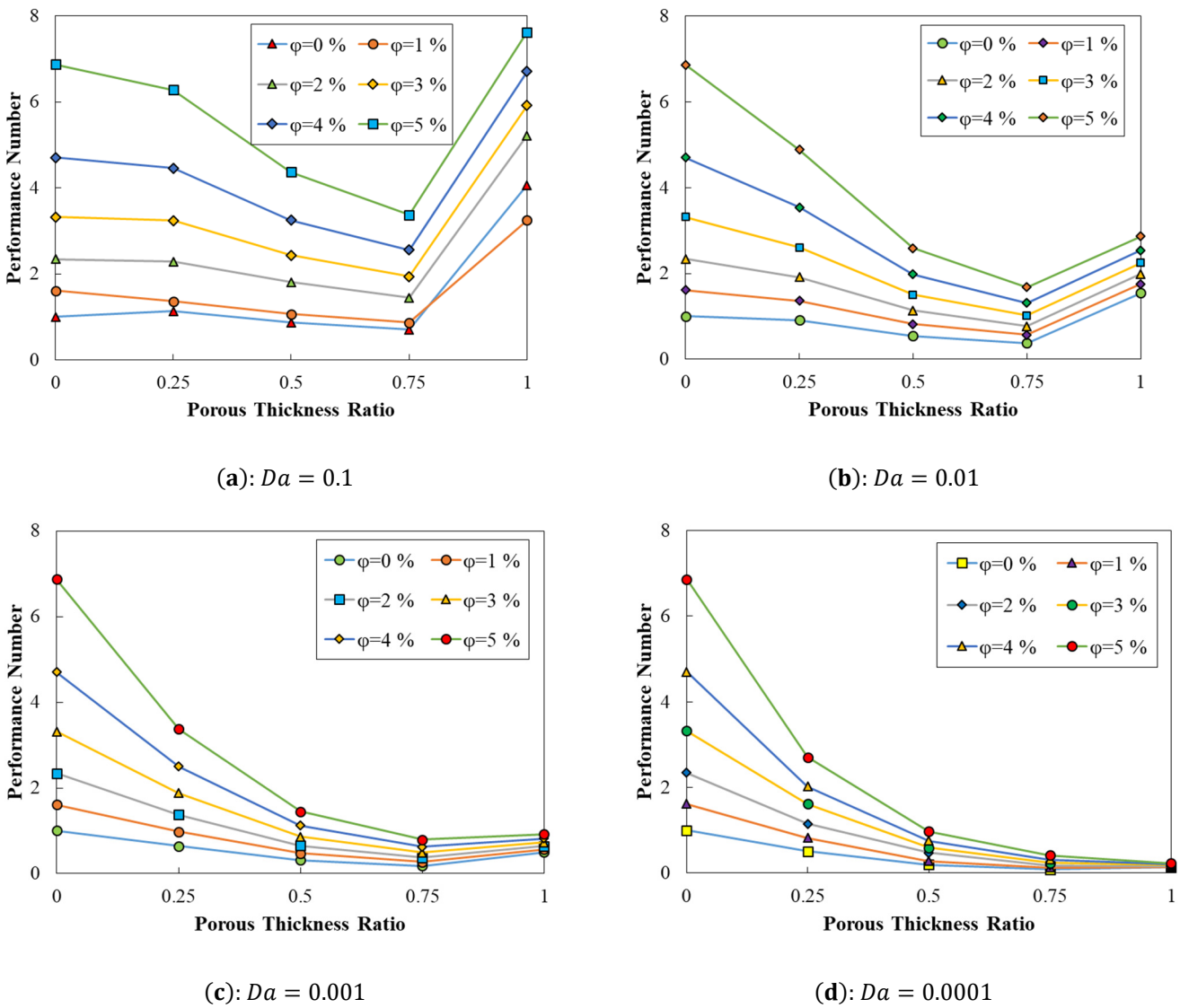

Figure 8. Performance number versus porous thickness ratio for diverse volume fraction at different Darcy numbers (case II).

For both cases I and II, PN revealed an increasing trend by rising the nanoparticles' concentration from 0% to 5%. By adding the hybrid nanofluid to the CMC and augmenting the volume fractions (from 0% to 5%), the thermal conductivity coefficient increases considerably, eventually leading to a better heat transfer. Moreover, as illustrated in Figures 7 and 8, the increased total Nusselt number can increase the PN as a result of the heat transfer coefficient's influence on the flow under a constant Darcy number. Furthermore, by comparing the results for both cases I and II, the greatest PN was found at $r_p = 1$, $\varphi = 5\%$, and $Da = 0.1$ ($PN = 7.61$). Additionally, according to the outcomes, for both cases I and II, in the presence of the hybrid nanofluid with a volume fraction of 5% at $Da = 0.1$ and $r_p = 1$, an augmented PN can be realized at almost 88% compared to the zero volume fraction.

4. Temperature Contours

Figure 9 shows the temperature contours for the two cases, with and without the addition of solid particles to the CMC and porosity for various Darcy numbers. As represented in Figure 9, using the nanofluid in combination with a porous medium enhanced the heat transfer. However, according to Figure 9a, the temperature is uniformly distributed in the absence of a porous medium.

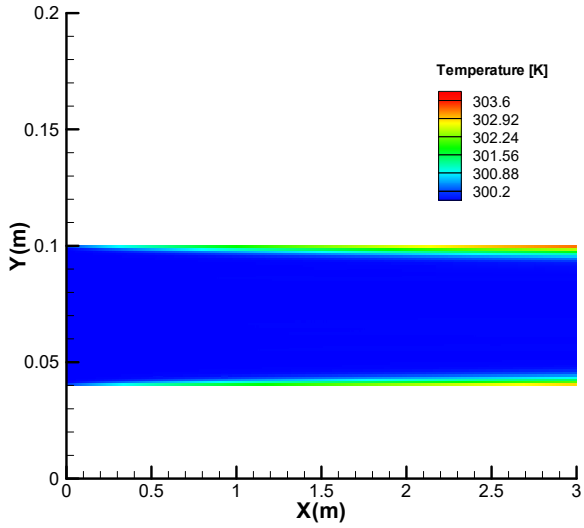

(**a**): $Base\ Fluid, \quad \varphi = 0\%$

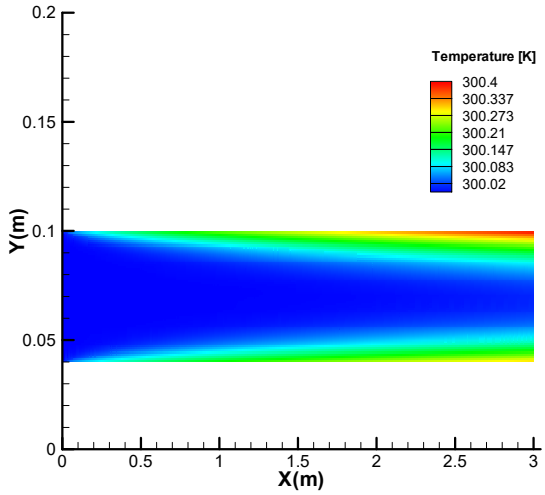

(**b**): $Da = 0.1\,, \quad \varphi = 1\%$

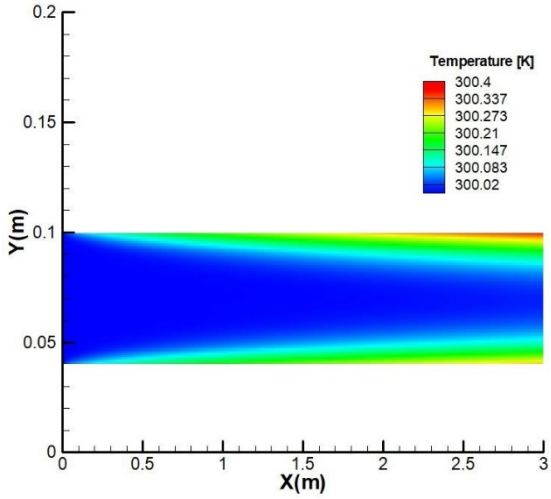

(**c**): $Da = 0.01, \quad \varphi = 1\%$

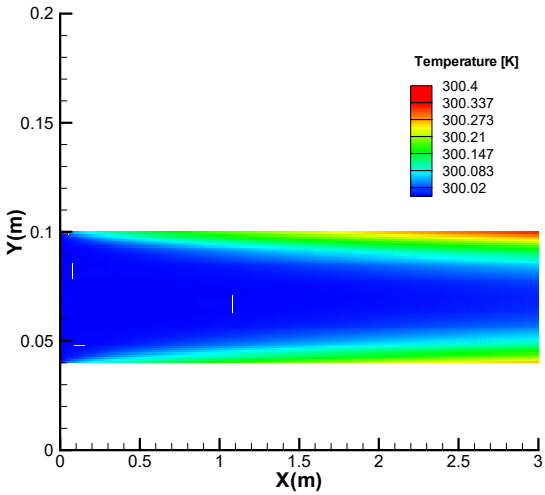

(**d**): $Da = 0.001, \quad \varphi = 1\%$

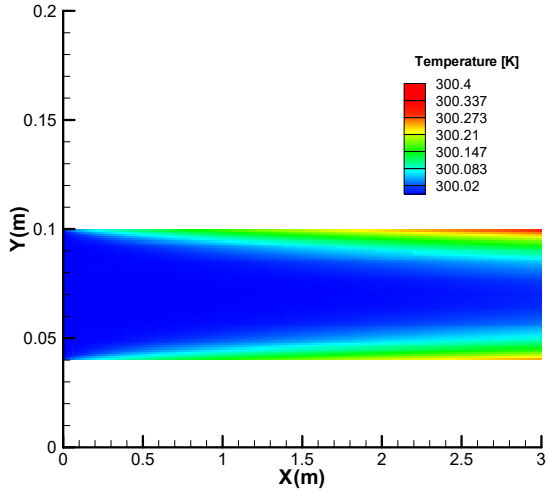

(**e**): $Da = 0.0001, \quad \varphi = 1\%$

Figure 9. Temperature contours for diverse Darcy numbers utilizing CMC and hybrid nanofluid at different Darcy numbers, considering ($r_p = 1$).

Lowering the Darcy number from 0.1 to 0.0001 reduces the thermal boundary layer thickness and, consequently, improves the heat transfer. Therefore, in the medium with low permeability as well as in the presence of a nanofluid ($\varphi \neq 0$), the temperature gradient close to the walls increases.

5. Conclusions

In the present work, the (Al_2O_3-CuO + CMC) non-Newtonian hybrid nanofluid was numerically used to improve laminar forced convection within an annular pipe and in a porous medium inserted into its outer or inner wall. The annular pipe walls were exposed to a constant heat flux. The non-Newtonian hybrid nanofluid flow was modeled using the Darcy–Brinkman–Forchheimer formulation for describing the fluid flow in the porous medium. The commercial CFD code ANSYS-FLUENT, which is based on the finite volume method, was utilized to solve the governing equations and to examine the influence of several major variables (such as volume fraction and Darcy number) on the heat transfer as well as pressure drop. Moreover, a new parameter, namely, the performance number (PN), was introduced in this study as a measure to further investigate the systems' thermal performance. The following points can be concluded:

- By reducing the Darcy number (from 0.1 to 0.0001) and increasing the thickness ratio of the porosity, the total Nusselt number rises.
- The heat transfer coefficient and total Nusselt number could be enhanced by incorporating metal nanoparticles into the CMC base fluid. Based on the results, at a constant porous thickness ratio and Darcy number ($r_p = 1, Da = 0.0001$), as well as at a volume fraction of 5%, the maximum total Nusselt number reached 1274.44 for both cases I and II. Moreover, increasing the volume fraction to an optimal value of 5%, considering $Da = 0.0001$ and $r_p = 1$, leads to an improvement in the total Nusselt number of approximately 14% for both cases I and II, in comparison to that with no usage of nanoparticles.
- Increasing the Darcy number lowers the pressure drop at a constant volume fraction.
- The pressure drop increased under the constant Darcy number by rising the porous thickness ratio.
- For the two cases I and II, which refer to the porous insert being situated in the inner and outer wall, respectively, the total Nusselt number and PN revealed an increasing pattern by augmenting the nanoparticles' volume fraction from 0% to 5% in comparison to the CMC base fluid due to its thermophysical properties.
- Augmenting the Darcy number could enhance the PN. Additionally, regarding permeable porous media ($Da = 0.1$ and $r_p = 1$), a maximum value for the PN can be obtained ($PN = 7.61$). Furthermore, based on the outcomes for both cases I and II, by increasing the volume fraction of the nanoparticles to 5% at $Da = 0.1$ and $r_p = 1$, an augmented PN can be realized of around 88% compared to the zero volume fraction.

It should be noted that studying the different non-Newtonian hybrid nanofluids impacts on forced convection by considering complex arrangements in porous media, investigating the impacts of particles' size and shape, and developing the model to include the diverse hybrid nanofluid viscosity should be considered in future works.

Author Contributions: Conceptualization, H.M. and E.A.; methodology, H.M. and E.A.; software, E.A.; investigation, H.M., E.A., M.B. (Mohamad Bayat) and M.B. (Mahdi Bodaghi); data curation, E.A.; writing—original draft preparation, H.M.; writing—review and editing, H.M., M.B. (Mohamad Bayat) and M.B. (Mahdi Bodaghi); supervision, J.H.H. and M.B. (Mahdi Bodaghi); project administration, J.H.H. and M.B. (Mahdi Bodaghi). All authors have read and agreed to the published version of the manuscript.

Funding: This research did not receive any specific grant from funding agencies in the public, commercial, or not-for-profit sectors.

Data Availability Statement: Not applicable. The authors declare that the paper is a product of our original research investigation.

Conflicts of Interest: The authors declare that they have no known competing financial interests or personal relationships that could have appeared to influence the work reported in this paper.

Nomenclature

C	Specific heat/J·kg^{-1}·K^{-1}
D	Pipe diameter/m
g	Gravity acceleration/m·s^{-2}
K	Porous medium permeability/m^2
k	Thermal conductivity/W·m^{-1}·K^{-1}
L	Length/m
m	Consistency index
n	Power-law index
P	Nondimensional pressure
p	Pressure/Pa
q''	Heat flux/W·m^{-2}
R	Pipe radius/m
R_p	Porous substrate thickness/m
r_p	Porous thickness ratio
T	Temperature/K
U	Velocity component/m·s^{-1}
x, y	Dimensional coordinates/m
Greek symbols	
$\dot{\gamma}$	Shear rate/s^{-1}
ε	Porosity
μ	Dynamic viscosity/kg·m^{-1}·s^{-1}
ρ	Density/kg·m^{-3}
φ	Volume fraction
Subscripts	
b	Base
bf	Base fluid
eff	Effective
f	Fluid
i	Inner
in	Inlet
hnf	Hybrid nanofluid
m	Mixture
nf	Nanofluid
np	Nanoparticles
o	Outer
p	Porous
Abbreviations	
2D	Two-dimensional
CFD	Computational fluid dynamics
CMC	Carboxy methyl cellulose
Da	Darcy number
FVM	Finite volume method
Nu	Nusselt number
PN	Performance number
Re	Reynolds number
SIMPLE	Semi-implicit method for pressure-linked equations

References

1. Ahmadi, A.A.; Khodabandeh, E.; Moghadasi, H.; Malekian, N.; Akbari, O.A.; Bahiraei, M. Numerical study of flow and heat transfer of water-Al_2O_3 nanofluid inside a channel with an inner cylinder using Eulerian–Lagrangian approach. *J. Therm. Anal. Calorim.* **2018**, *132*, 651–665. [CrossRef]
2. Farhangmehr, V.; Moghadasi, H.; Asiaei, S. A nanofluid MHD flow with heat and mass transfers over a sheet by nonlinear boundary conditions: Heat and mass transfers enhancement. *J. Cent. South Univ.* **2019**, *26*, 1205–1217. [CrossRef]

3. Mousavi Ajarostaghi, S.S.; Zaboli, M.; Javadi, H.; Badenes, B.; Urchueguia, J.F. A review of recent passive heat transfer enhancement methods. *Energies* **2022**, *15*, 986. [CrossRef]
4. Malekian, S.; Fathi, E.; Malekian, N.; Moghadasi, H.; Moghimi, M. Analytical and numerical investigations of unsteady graphene oxide nanofluid flow between two parallel plates. *Int. J. Thermophys.* **2018**, *39*, 100. [CrossRef]
5. Ghanbari, K.; Golneshan, A.A.; Yazdani, M.; Moghadasi, H.; Malekian, N. An experimental study of forced convective heat transfer for fully developed Al_2O_3–water nanofluid in an annulus tube. *Heat Transf.* **2021**, *50*, 5697–5713. [CrossRef]
6. Cieśliński, J.T. Numerical Modelling of Forced Convection of Nanofluids in Smooth, Round Tubes: A Review. *Energies* **2022**, *15*, 7586. [CrossRef]
7. Yang, L.; Ji, W.; Mao, M.; Huang, J.-n. An updated review on the properties, fabrication and application of hybrid-nanofluids along with their environmental effects. *J. Clean. Prod.* **2020**, *257*, 120408. [CrossRef]
8. Moghadasi, H.; Aminian, E.; Saffari, H.; Mahjoorghani, M.; Emamifar, A. Numerical analysis on laminar forced convection improvement of hybrid nanofluid within a U-bend pipe in porous media. *Int. J. Mech. Sci.* **2020**, *179*, 105659. [CrossRef]
9. Saghir, M.; Rahman, M. Forced convection of Al_2O_3–Cu, TiO_2–SiO_2, FWCNT–Fe_3O_4, and ND–Fe_3O_4 hybrid nanofluid in porous media. *Energies* **2020**, *13*, 2902. [CrossRef]
10. Gowda, R.P.; Kumar, R.N.; Aldalbahi, A.; Issakhov, A.; Prasannakumara, B.; Rahimi-Gorji, M.; Rahaman, M. Thermophoretic particle deposition in time-dependent flow of hybrid nanofluid over rotating and vertically upward/downward moving disk. *Surf. Interfaces* **2021**, *22*, 100864. [CrossRef]
11. Li, Y.-X.; Khan, M.I.; Gowda, R.P.; Ali, A.; Farooq, S.; Chu, Y.-M.; Khan, S.U. Dynamics of aluminum oxide and copper hybrid nanofluid in nonlinear mixed Marangoni convective flow with entropy generation: Applications to renewable energy. *Chin. J. Phys.* **2021**, *73*, 275–287. [CrossRef]
12. Tahir, S.; Mital, M. Numerical investigation of laminar nanofluid developing flow and heat transfer in a circular channel. *Appl. Therm. Eng.* **2012**, *39*, 8–14. [CrossRef]
13. Moshizi, S.; Malvandi, A.; Ganji, D.; Pop, I. A two-phase theoretical study of Al_2O_3–water nanofluid flow inside a concentric pipe with heat generation/absorption. *Int. J. Therm. Sci.* **2014**, *84*, 347–357. [CrossRef]
14. Suresh, S.; Venkitaraj, K.; Selvakumar, P.; Chandrasekar, M. Synthesis of Al_2O_3–Cu/water hybrid nanofluids using two step method and its thermo physical properties. *Colloids Surf. A Physicochem. Eng. Asp.* **2011**, *388*, 41–48. [CrossRef]
15. Moghadassi, A.; Ghomi, E.; Parvizian, F. A numerical study of water based Al_2O_3 and Al_2O_3–Cu hybrid nanofluid effect on forced convective heat transfer. *Int. J. Therm. Sci.* **2015**, *92*, 50–57. [CrossRef]
16. Emamifar, A.; Moghadasi, H.; Noroozi, M.J.; Saffari, H. Transient analysis of convective-radiative heat transfer through porous fins with temperature-dependent thermal conductivity and internal heat generation. *J. Therm. Eng.* **2021**, *8*, 656–666. [CrossRef]
17. Habibishandiz, M.; Saghir, M. A critical review of heat transfer enhancement methods in the presence of porous media, nanofluids, and microorganisms. *Therm. Sci. Eng. Prog.* **2022**, *30*, 101267. [CrossRef]
18. Uphill, S.J.; Cosgrove, T.; Briscoe, W.H. Flow of nanofluids through porous media: Preserving timber with colloid science. *Colloids Surf. A Physicochem. Eng. Asp.* **2014**, *460*, 38–50. [CrossRef]
19. Sundar, L.S.; Singh, M.K.; Sousa, A.C. Enhanced heat transfer and friction factor of MWCNT–Fe_3O_4/water hybrid nanofluids. *Int. Commun. Heat Mass Transf.* **2014**, *52*, 73–83. [CrossRef]
20. Esfe, M.H.; Wongwises, S.; Naderi, A.; Asadi, A.; Safaei, M.R.; Rostamian, H.; Dahari, M.; Karimipour, A. Thermal conductivity of Cu/TiO_2–water/EG hybrid nanofluid: Experimental data and modeling using artificial neural network and correlation. *Int. Commun. Heat Mass Transf.* **2015**, *66*, 100–104. [CrossRef]
21. Targui, N.; Kahalerras, H. Analysis of a double pipe heat exchanger performance by use of porous baffles and nanofluids. *Int. J. Mech. Aerosp. Ind. Mechatron. Manuf. Eng.* **2014**, *8*, 1581–1586.
22. Ajeeb, W.; Oliveira, M.S.; Martins, N.; Murshed, S.S. Performance evaluation of convective heat transfer and laminar flow of non-Newtonian MWCNTs in a circular tube. *Therm. Sci. Eng. Prog.* **2021**, *25*, 101029. [CrossRef]
23. Naveen Kumar, R.; Gowda, R.; Gireesha, B.; Prasannakumara, B. Non-Newtonian hybrid nanofluid flow over vertically upward/downward moving rotating disk in a Darcy–Forchheimer porous medium. *Eur. Phys. J. Spec. Top.* **2021**, *230*, 1227–1237. [CrossRef]
24. Sarada, K.; Gowda, R.J.P.; Sarris, I.E.; Kumar, R.N.; Prasannakumara, B.C. Effect of magnetohydrodynamics on heat transfer behaviour of a non-Newtonian fluid flow over a stretching sheet under local thermal non-equilibrium condition. *Fluids* **2021**, *6*, 264. [CrossRef]
25. Yang, L.; Du, K. A comprehensive review on the natural, forced, and mixed convection of non-Newtonian fluids (nanofluids) inside different cavities. *J. Therm. Anal. Calorim.* **2020**, *140*, 2033–2054. [CrossRef]
26. Hatami, M.; Ganji, D. Heat transfer and flow analysis for SA-TiO_2 non-Newtonian nanofluid passing through the porous media between two coaxial cylinders. *J. Mol. Liq.* **2013**, *188*, 155–161. [CrossRef]
27. Shahsavar, A.; Godini, A.; Sardari, P.T.; Toghraie, D.; Salehipour, H. Impact of variable fluid properties on forced convection of Fe_3O_4/CNT/water hybrid nanofluid in a double-pipe mini-channel heat exchanger. *J. Therm. Anal. Calorim.* **2019**, *137*, 1031–1043. [CrossRef]
28. Moraveji, M.K.; Haddad, S.M.H.; Darabi, M. Modeling of forced convective heat transfer of a non-Newtonian nanofluid in the horizontal tube under constant heat flux with computational fluid dynamics. *Int. Commun. Heat Mass Transf.* **2012**, *39*, 995–999. [CrossRef]

29. Miansari, M.; Aghajani, H.; Zarringhalam, M.; Toghraie, D. Numerical study on the effects of geometrical parameters and Reynolds number on the heat transfer behavior of carboxy-methyl cellulose/CuO non-Newtonian nanofluid inside a rectangular microchannel. *J. Therm. Anal. Calorim.* **2021**, *144*, 179–187. [CrossRef]
30. Aminian, E.; Moghadasi, H.; Saffari, H.; Gheitaghy, A.M. Investigation of forced convection enhancement and entropy generation of nanofluid flow through a corrugated minichannel filled with a porous media. *Entropy* **2020**, *22*, 1008. [CrossRef]
31. Al-Rashed, A.A.; Shahsavar, A.; Entezari, S.; Moghimi, M.; Adio, S.A.; Nguyen, T.K. Numerical investigation of non-Newtonian water-CMC/CuO nanofluid flow in an offset strip-fin microchannel heat sink: Thermal performance and thermodynamic considerations. *Appl. Therm. Eng.* **2019**, *155*, 247–258. [CrossRef]
32. Zainith, P.; Mishra, N.K. Experimental investigations on stability and viscosity of carboxymethyl cellulose (CMC)-based non-newtonian nanofluids with different nanoparticles with the combination of distilled water. *Int. J. Thermophys.* **2021**, *42*, 137. [CrossRef]
33. Aminian, E.; Moghadasi, H.; Saffari, H. Magnetic field effects on forced convection flow of a hybrid nanofluid in a cylinder filled with porous media: A numerical study. *J. Therm. Anal. Calorim.* **2020**, *141*, 2019–2031. [CrossRef]
34. Ashorynejad, H.R.; Shahriari, A. MHD natural convection of hybrid nanofluid in an open wavy cavity. *Results Phys.* **2018**, *9*, 440–455. [CrossRef]
35. Pordanjani, A.H.; Vahedi, S.M.; Aghakhani, S.; Afrand, M.; Öztop, H.F.; Abu-Hamdeh, N. Effect of magnetic field on mixed convection and entropy generation of hybrid nanofluid in an inclined enclosure: Sensitivity analysis and optimization. *Eur. Phys. J. Plus* **2019**, *134*, 412. [CrossRef]
36. Ramachandran, R.; Ganesan, K.; Rajkumar, M.; Asirvatham, L.; Wongwises, S. Comparative study of the effect of hybrid nanoparticle on the thermal performance of cylindrical screen mesh heat pipe. *Int. Commun. Heat Mass Transf.* **2016**, *76*, 294–300. [CrossRef]
37. Tahat, M.S.; Benim, A.C. Experimental analysis on thermophysical properties of Al_2O_3/CuO hybrid nano fluid with its effects on flat plate solar collector. *Defect Diffus. Forum* **2017**, *76*, 148–156. [CrossRef]
38. Saqib, M.; Khan, I.; Shafie, S. Natural convection channel flow of CMC-based CNTs nanofluid. *Eur. Phys. J. Plus* **2018**, *133*, 549. [CrossRef]
39. Akbari, O.A.; Toghraie, D.; Karimipour, A.; Marzban, A.; Ahmadi, G.R. The effect of velocity and dimension of solid nanoparticles on heat transfer in non-Newtonian nanofluid. *Phys. E Low-Dimens. Syst. Nanostruct.* **2017**, *86*, 68–75. [CrossRef]
40. Siavashi, M.; Bahrami, H.R.T.; Saffari, H. Numerical investigation of flow characteristics, heat transfer and entropy generation of nanofluid flow inside an annular pipe partially or completely filled with porous media using two-phase mixture model. *Energy* **2015**, *93*, 2451–2466. [CrossRef]